01 Jan 2023

Experimental Approach for Development of a Powder Spreading Metric in Additive Manufacturing

M. Hossein Sehhat

Austin T. Sutton

Zane Yates

Ming-Chuan Leu
Missouri University of Science and Technology, mleu@mst.edu

Recommended Citation

M. H. Sehhat et al., "Experimental Approach for Development of a Powder Spreading Metric in Additive Manufacturing," *International Journal of Advanced Manufacturing Technology*, Springer, Jan 2023.
The definitive version is available at https://doi.org/10.1007/s00170-023-11120-x

The International Journal of Advanced Manufacturing Technology
https://doi.org/10.1007/s00170-023-11120-x

ORIGINAL ARTICLE

Experimental approach for development of a powder spreading metric in additive manufacturing

M. Hossein Sehhat[1] · Austin T. Sutton[2] · Zane Yates[1] · Ming C. Leu[1]

Received: 7 December 2022 / Accepted: 15 February 2023

Abstract
The powder spreading is a vital step of powder-based additive manufacturing (AM) processes. The quality of spread powder can considerably influence the properties of fabricated parts. Poorly packed powder beds with high surface roughness result in printed part layers with large porosity and low dimensional accuracy, leading to poor mechanical properties. Therefore, the powder spreadability and its dependence on process parameters and powder characteristics should be quantified to improve the efficiency of powder-based AM methods. This study proposes a novel dimensionless powder spreadability metric that can be commonly used in different powder-based AM processes. The quality of spread powder in terms of powder bed density and surface roughness was evaluated by adjusting the process parameters including recoating velocity and layer thickness, and powder characteristics including particle size distribution. In addition, the dynamic repose angle was proposed and examined as another powder spreadability metric. The results showed that these two proposed metrics were strongly correlated and lower recoating velocity and larger layer thickness led to higher spreadability and lower dynamic repose angle.

Keywords Powder spreading · Powder bed density · Powder surface roughness · Dynamic repose angle · Design of experiments (DOE) · Additive manufacturing

1 Introduction

The conventional manufacturing methods include many steps such as machining, forming, assembling, and welding. [1–6]. The material and part handling among these steps can be very time-consuming in addition to the time and labor cost each of these steps takes to proceed with the production process. The advent of additive manufacturing (AM) decreased the need for several of these steps as it fabricates the parts in a single-step layer-based manufacturing fashion [4, 7, 8]. In AM processes, the part geometry data is sliced into several layers and is given to the AM machine. The material feedstock will be used to fabricate each part's layer. The final component is fabricated by repeating the material injection and production process for all part's layers [9]. Due to this layer-by-layer manufacturing process, the fabrication of high-complex geometry components with high accuracy and desirable part properties is possible [10, 11].

Depending on the type of AM process, the format of material feedstock is different. For instance, laser foil printing (LFP) uses metal foils while Ceramic On-Demand Extrusion uses paste, and fused deposition modeling (FDM) uses filaments [12–18]. The powder is another widespread material format in AM, especially in powder-based AM processes [19–21]. Due to the higher formability of powder material, it is beneficial in fabricating parts with highly complicated geometries [22]. However, the specific fabrication conditions of AM, such as the creation of very thin layers, may adversely affect the powder characteristics and consequently deteriorate the powder performance in terms of powder spreadability. In addition, the process temperature should be accordingly controlled to avoid creation of defects in fabricated parts [23–25], and collision between fabricated part layers and powder recoater, which can be considered as a two fixed end beam [26].

The first step of fabricating each part's layer in powder-based AM methods is delivering the powder feedstock. As the delivered powder contributes to the fabrication of a single layer at a time, it should be deposited on the build plate

✉ M. Hossein Sehhat
hsehhat@mst.edu

[1] Department of Mechanical and Aerospace Engineering, Missouri University of Science and Technology, Rolla, MO 65409, USA

[2] Los Alamos National Laboratory, Los Alamos, NM 87545, USA

Published online: 25 February 2023

(substrate) with the thickness of a part's layer. Although some techniques such as decreasing the part's surface roughness by adjusting layer thickness for different layers have been implemented to improve the part's quality, the properties of the spread powder layer may influence the quality of fabricated parts [27–30]. Each powder layer should be highly dense with low surface roughness to result in the desired part features including low porosity, high mechanical properties, and high dimensional accuracy [31–34]. Also, the powder should be rapidly delivered for each part's layer to minimize the fabrication time and maximize the process efficiency. Thus, the powder should be spread with a specific layer thickness (LT) and recoating velocity (RV) to quickly create a dense powder layer with low surface roughness.

Many researchers in recent years have studied powder spreadability and its dependence on spreading process parameters. As no spreadability metric was commonly used in the AM community, the researchers proposed some spreadability metrics and examined their validity. These spreadability metrics have been reported and extensively discussed in a comprehensive review paper by Sehhat et al. [35]. The observed empty areas on the substrate with various LTs were reported by Ahmed et al. [36]; they found that the lower layer thicknesses resulted in a greater number of empty areas in the substrate. Cordova et al. [37] proposed the relative density as the powder spreadability metric, defined as the ratio of apparent density over material density (ρ), and the relative density was evaluated in two different recoater designs. The funnel recoater, in which the particles were pushed down by the gravity forces of overhead particles, deposited a greater number of particles in the substrate and resulted in a higher relative density as the gravity forces dominated the Van der Waals forces among particles. Zhang et al. [38] considered the powder bed density as a powder spreadability metric; they found that powder bed density deteriorates at high RV and low LT due to powder splash and particle jamming, respectively. Surface roughness of spread powder was considered as a spreadability metric in a study by Parteli et al. [39], where higher RV resulted in larger surface roughness, i.e., lower spreadability.

Although several spreadability metrics have been proposed and investigated in the literature, the existence of a dimensionless powder spreadability metric that can be commonly used in different AM processes is still lacking. In this study, powder performance in terms of powder bed density and surface roughness was assessed, and a dimensionless powder spreadability metric was proposed based on them. To evaluate the powder spreadability as a metric independent on the material characteristics, the measured density of the spread layer (measured mass (m)/computed volume (v)) was divided by the material density, ρ, and the resulting quantity was called powder bed density. Also, the measured surface roughness (Ra) was divided by the medium particle size of powder, D_{50}, and the resulting quantity was called relative roughness, which is independent of the powder particles size. Since it is desired for the spread powder layers to be dense with little roughness, the powder bed density was divided by the relative roughness to create a dimensionless ratio that increases with improved powder bed quality. Thus, powder spreadability is defined as

$$Spreadability = \frac{Powder\ Bed\ Density}{Relative\ Roughness} = \frac{\left(\frac{\left(\frac{m}{v}\right)}{\rho}\right)}{\left(\frac{R_a}{D_{50}}\right)} = \frac{m.D_{50}}{v.\rho.R_a}$$

In addition, another powder spreadability metric, dynamic repose angle (DRA), was proposed and measured by the side view images obtained by the high-speed camera. Powders with higher flowability are known to result in smaller magnitudes of the angle of repose [40] similar to the flow behavior of granular material [41]. In a similar approach, smaller magnitudes of DRA indicate higher powder spreadability. The influence of spreading process parameters, including RV and LT, and powder characteristics, including particle size distribution (PSD), on these proposed spreadability metrics was evaluated. The trends for obtaining higher powder spreadability were determined. While in several research studies in the literature the researchers sufficed with the low-accuracy results of powder spreading manually with their hands, in this work, we report the high-accuracy results of powder spreading provided by an in-house fabricated automatic high-accuracy spreading setup.

The rest of this paper is organized as follows. Section 2 provides the information on the used material and the fabricated spreading setup for performing spreadability experiments. Section 3 discusses the impact of RV, LT, and PSD on powder spreadability and DRA, followed by the correlation relationship between them.

2 Material and methods

2.1 Material

The gas-atomized AISI 304L stainless steel powder was provided by LPW Technology (Carpenter Technology Corporation, USA). The manufacturer reported the powder density as 2.7 g/cm^3 and the powder particle size distribution as 13, 20, and 30 µm for D_{10}, D_{50}, and D_{90}, where D_{10}, D_{50}, and D_{90} are the 10th, 50th, and 90th percentiles, respectively, of the particle size distribution. As the particle size distribution will be discussed in the following sections, the powder size span can be used as a meaningful representative of powder PSD. The powder size span can be defined as

$$Span = \frac{D_{90} - D_{10}}{D_{50}}$$

with its larger values indicating higher PSD.

2.2 Fabrication of the powder spreading setup

Fabrication of an automatic high-accuracy and high-resolution spreading system was required to accurately study the different properties of the powder bed. Figure 1 shows the fabricated powder spreading setup with major components of a 3D gantry system, a laser line profiler, and a high-speed camera. The automatic gantry system is controlled with a computer numerical control (CNC) program and can provide a high motion resolution of 1 µm. The function of the gantry system is to move the powder recoater over the static table to spread the powder on the substrate, move the laser profiler over the spread powder layer to scan the coordinates of the spread layer, and move the high-speed camera for measurement of DRA.

The deployed laser line profiler is a Gocator 2320 (LMI Technologies Inc., Canada) with a resolution of 1.8–3 µm in the *Z* direction and 14–21 µm in the *X* direction. It can provide coordinate information of 1280 data points per laser profile. By processing the obtained data points in the Mountains Map® software (Digital Surf, France), the required properties of the spread powder layer, such as volume and surface roughness, were computed.

The high-speed camera is an SC1 Edgertronic (Sanstreak Corp, USA) capable of capturing 700 frames per second (fps) at a resolution of 1280 × 720 pixels. The provided high fps of this camera makes the in situ capture of powder DRA possible during the powder spreading process. The camera is attached to the recoater's side and moves with it, i.e., although the camera is moving relative to the static table, the camera is static relative to the recoater's side. Thus, during the spreading process, the camera is watching a still frame of powder spreading with a changing powder DRA.

2.3 Design of experiments

The goal was to evaluate the impact of spreading process parameters on powder properties. The variable factors were recoating velocity (RV), layer thickness (LT), and particle size distribution (PSD). RV had 4 levels of 25% (32.5 mm/s), 50% (65 mm/s), 75% (97.5 mm/s), and 100% (130 mm/s). LT had 3 levels of 30, 50, and 70 µm. The virgin powder in its as-purchased condition was considered as one level of PSD (unsieved), and it was sieved by 45- and 25-µm screens to create the second level of PSD, including particles smaller than 45 µm but larger than 25 µm (25 < PSD < 45, hereafter called 25–45). Also, to distinctly investigate the impact of particle size (PS) on powder spreadability, three PSs of smaller than 25 µm (PS < 25 µm, hereafter called < 25), 25–45, and larger than 45 µm (45 < PS, hereafter called > 45) were studied. The particle size information of these three powder sizes is shown in Table 1. Adjustment of RV and LT was performed through the CNC program of the gantry system. The studied powder properties such as powder bed density, powder surface roughness, and powder DRA were considered as response variables. To evaluate the results' repeatability, each experiment was replicated three times, and their mean and standard deviations were reported.

Table 1 The particle size and distribution of experimented powder samples

Particle size	D_{10} (µm)	D_{50} (µm)	D_{90} (µm)	Span (dimensionless)
< 25	12.57	17.71	25.23	0.71
25–45	20.41	28.70	39.78	0.67
> 45	32.42	43.27	56.43	0.56
Unsieved	20.57	29.80	47.45	0.90

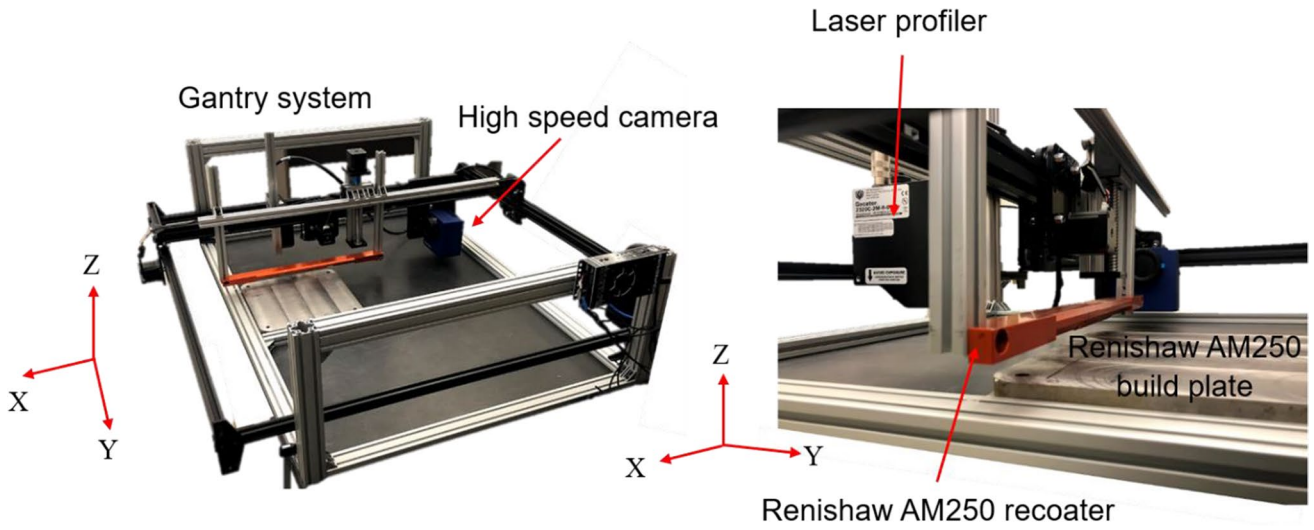

Fig. 1 Fabricated powder spreading setup

The powder bed density was defined as the mass over the volume of spread powder. The powder mass was measured for each spreading experiment before spreading the powder on the substrate. To measure the volume of spread powder, the laser profiler should scan all the spread powder's top surface. Based on the point cloud obtained by the laser profiler, the MountainsMap® software computed the volume, which would be the volume of space between the substrate and the scanned point cloud of powder layer. Then, the powder bed density was obtained by dividing the measured mass over the computed volume.

The powder surface roughness was measured by the MountainsMap® software. Figure 2a is an instance of the top view of a powder layer spread with RV 25% and LT 30 µm. The software can generate the surface roughness Ra parameter for each scanned profile. As shown in Fig. 2b, for measurement of surface roughness per spreading experiment, 12 profiles (with 10-mm gap distance) of the scanned surface were selected, and their individual Ra was measured. Then, the mean and standard deviation of these 12 Ra values were reported as powder layer's surface roughness.

To assess the impact of RV on the powder layers spread with a constant LT 30, the values of surface roughness at a representative location along the spreading direction Y60 are shown in Table 2. Increasing the RV resulted in a layer with higher surface roughness.

The increased surface roughness when increasing RV can be observed in the surface profiles of corresponding spread layers with a constant LT 30 in the middle of the spread layer (Y60), as shown in Fig. 3.

In addition, to evaluate the impact of LT on powder layers spread with a constant RV 100, the values of surface roughness at a representative location along the spreading

Table 2 Impact of recoating velocity on surface roughness of powder layers spread with a constant layer thickness of 30 µm

Recoating velocity (%)	Ra (µm)
25	1.54
50	1.75
75	1.86
100	1.96

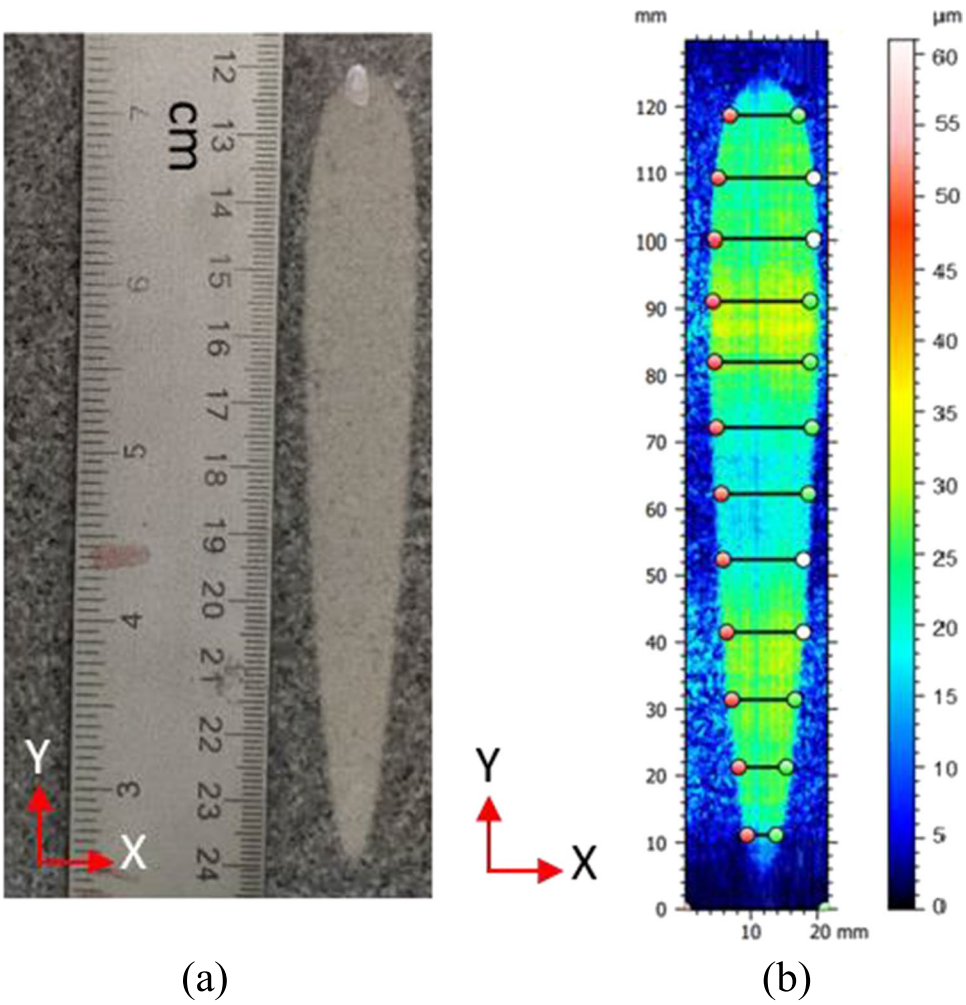

Fig. 2 An instance of the spread powder (spreading parameters: RV = 25% and LT = 30 µm). **a** Top-view of the spread layer and **b** 12 chosen profiles for measurement of Ra

direction Y60 are shown in Table 3. The surface roughness of the spread layer slightly decreased when using larger LTs; this is mainly because the powder particles are packed to the larger underneath material thickness.

The powder DRA was evaluated through performing image analysis on the side images obtained by the high-speed camera. Figure 4 shows an instance of the powder spreading process as watched by the high-speed camera. Figure 4a shows the powder released on the substrate in front of the recoater before spreading; the camera's view of this outlook is shown in Fig. 4b. As the spreading starts and the recoater makes contact with the powder, the powder pile is forced to move, which causes the creation of DRA in the powder pile. Figure 4c shows an instance of powder pile reaction during the spreading process, and the part of images used for DRA measurement is shown with a white rectangle. A closer look of the marked DRA can be seen in Fig. 4d. The ImageJ software [42] was used to measure the DRA angle between powder and substrate (α). For measurement of DRA per spreading experiment, 12 frames of the spreading process at the same locations of the 12 Ra profiles were investigated in image analysis. The angle in each frame was measured 10 times, and their mean was reported as the DRA for that specific frame. Then, the

Table 3 Impact of layer thickness on surface roughness of powder layers spread with a constant recoating velocity of 100%

Layer thickness (μm)	Ra (μm)
30	1.59
50	1.57
70	1.54

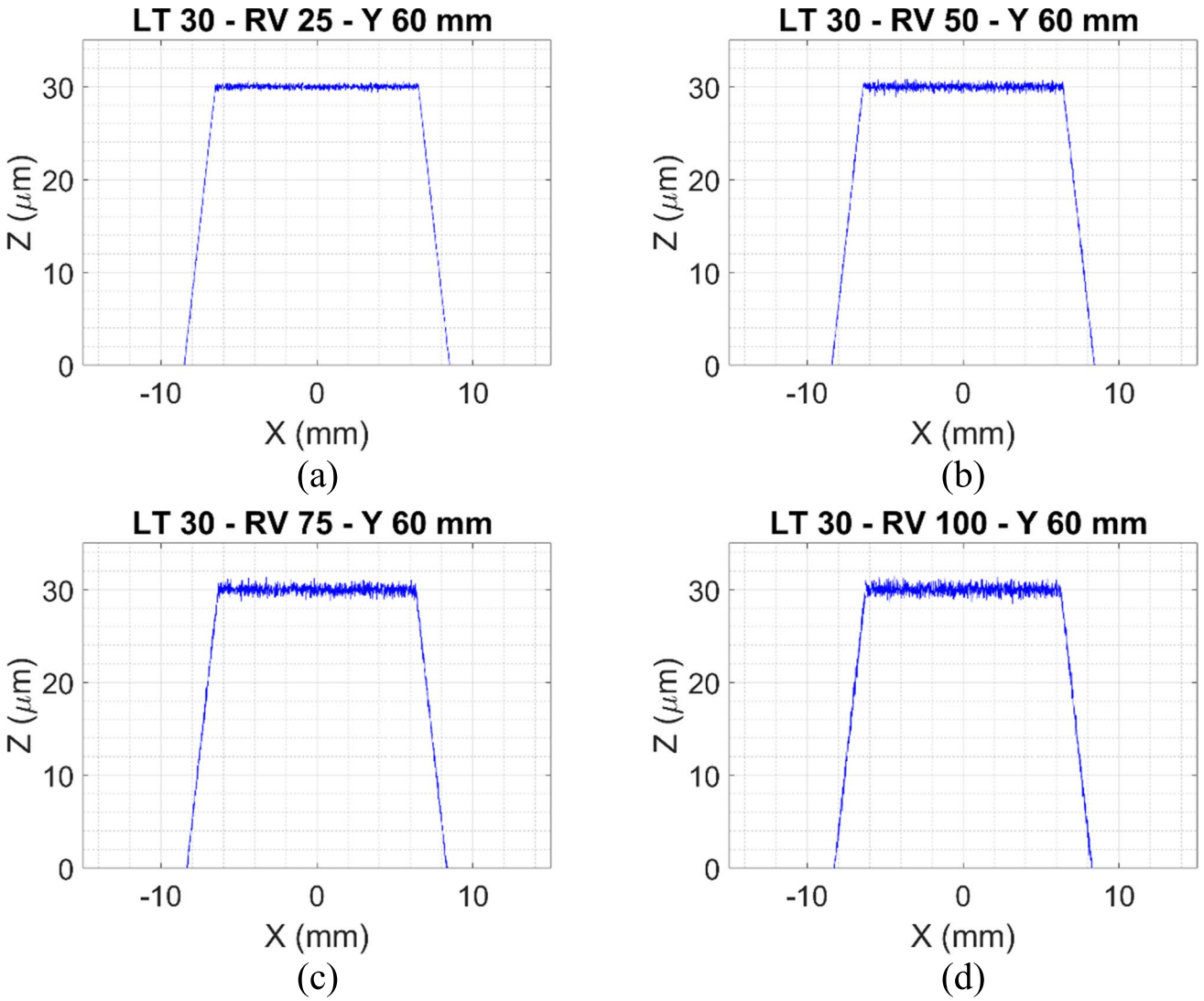

Fig. 3 Impact of RV on surface profiles of powder layers spread with a constant LT 30 at the middle of spread layer Y60. **a** RV 25, **b** RV 50, **c** RV 75, and **d** RV 100

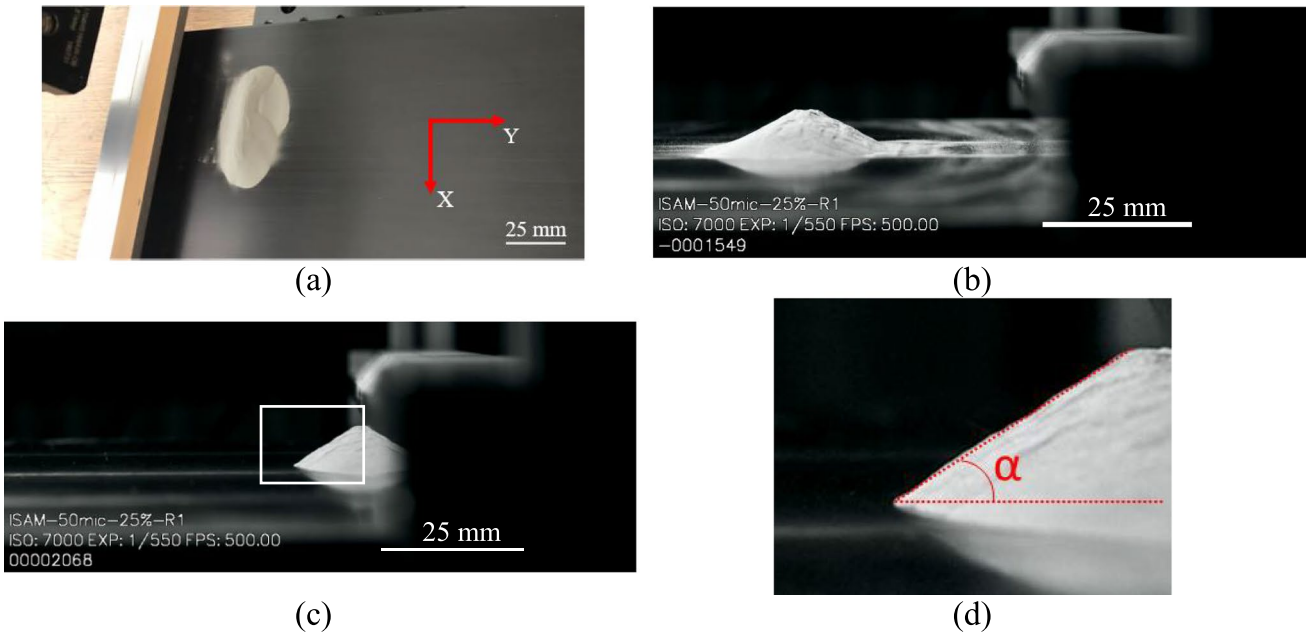

Fig. 4 Side view images of powder spreading obtained by high-speed camera: **a** released powder on the substrate before the start of spreading process, **b** before the recoater contacts the powder pile (recoater is moving to the left to spread the powder pile), **c** after recoater contacts and spreads the powder pile (the selected area for measurement of dynamic repose angle is marked), and **d** closer view of measurement area with marked powder dynamic repose angle

mean of these 12 DRAs (from 12 frames) was reported as the DRA per spreading experiment.

3 Results and discussion

3.1 Spreadability

3.1.1 Impact of recoating velocity (RV) and layer thickness (LT) on spreadability

Figure 5 illustrates the influence of RV and LT on powder spreadability. Increasing the RV from 25 to 100% considerably decreased the powder spreadability, while increasing LT from 30 to 70 µm had a marginal impact on the powder spreadability. This behavior can be explained by the increased momentum of particles at higher RV; as the particles are being pushed faster, they maintain their gained speed for a longer distance and in an arbitrary direction. This unorganized particle motion causes particles to deposit at random locations, creating empty areas in the substrate and leaving empty space among particles which then will be transformed to porosity in the fabricated LPBF parts.

Running an analysis of variance (ANOVA) with a significance level of 0.05 showed that the results of different experimental runs were significantly different (P-value < 0.0001).

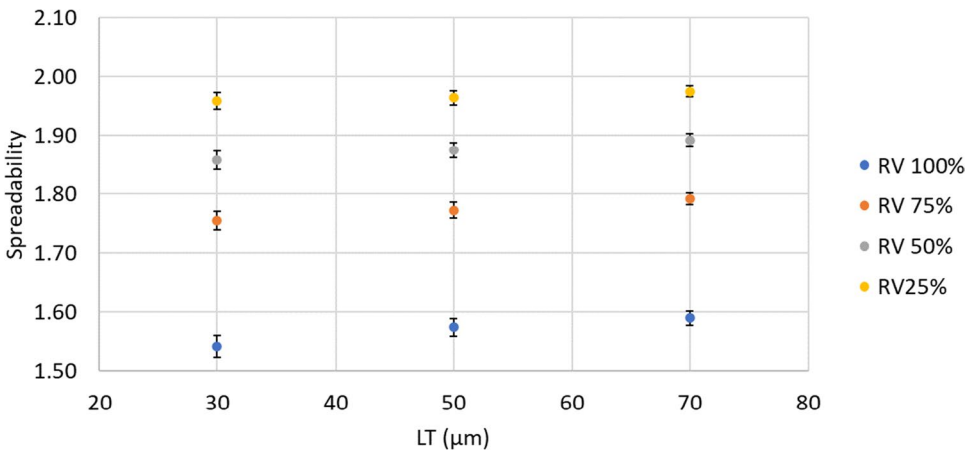

Fig. 5 Impact of recoating velocity and layer thickness on powder spreadability

No significant interaction was found between the RV and LT (Table 4); they were independent factors and the effect of RV on spreadability remained the same irrespective of the used LT. Looking at the main effects of each factor, both RV and LT are significant factors as their *P*-values of < 0.0001 and 0.0025, respectively, were smaller than the 0.05 significance level.

3.1.2 Impact of particle size (PS) and particle size distribution (PSD) on spreadability

To assess the effect of PS on powder spreadability, some experiments with a constant RV of 100% and LT of 50 µm were performed with three different PS of − 25, 25 − 45, and + 45 µm. The results of powder spreadability for this set of experiments are shown in Fig. 6. The particles larger than 45 µm (+ 45) showed the highest spreadability, and the spreadability decreased by decreasing the particle size. Also, decreasing the particle size led to larger deviations in powder spreadability. This relation between particle size and powder spreadability can be explained by the dimensionless "bonding number (*K*)" [35], where for a constant density the larger particles have higher gravity forces which outweigh the Van der Waals forces present among particles. As a result, the larger particles are less likely to agglomerate and are more willing to deposit in the substrate. On the other hand, the smaller particles have lower gravity forces, larger surface/mass ratio, and larger Van der Waals forces. Thus, for smaller particles, the Van der Waals forces outweigh the gravity force and cause the powder to agglomerate and act more cohesively, which is detrimental to powder spreadability.

For evaluating the effect of PSD on powder spreadability, only the extremum PSDs of the unsieved powder (with the widest PSD) and the 25–45 (sieved) powder (with the narrowest PSD) were studied. Figure 7 shows the relationship between span and powder spreadability for both unsieved and 25–45 powders. The narrow size span of 25–45 powder indicates that the particles are more uniform without large size variations, while the large span of unsieved powder indicates that the powder is composed of non-uniform particles with various sizes; although this size non-uniformity may intuitively sound helpful for creating denser powder layers by smaller particles filling the voids among larger particles, the whole powder's increased surface/mass ratio

Table 4 Evaluation of interaction term and main effects of recoating velocity and layer thickness on powder spreadability

Source	DF	Sum of squares	*F* ratio	Prob > *F*
LT (um)	2	0.00210753	7.7889	0.0025*
RV (%)	3	0.78379639	1931.151	< .0001*
LT (um)*RV (%)	6	0.00046873	0.5774	0.7445

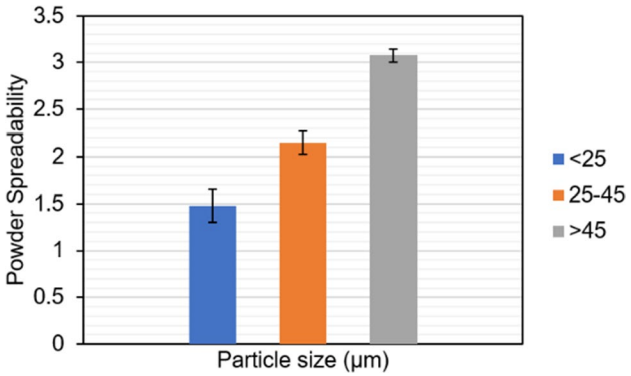

Fig. 6 Impact of particle size on powder spreadability

and the great magnitude of Van der Waals forces among these non-uniform particles deteriorated the powder bed density and surface roughness [37, 43]. Therefore, as the 25–45 powder had the narrowest size span, it showed higher spreadability than unsieved powder.

3.2 Dynamic repose angle (DRA)

3.2.1 Impact of recoating velocity (RV) and layer thickness (LT) on dynamic repose angle (DRA)

Figure 8 shows the impact of RV and LT on DRA. Increasing the RV resulted in larger DRAs as the particles are forced to move and repose in a shorter time. This faster velocity also increases the particles' momentum, forcing them to move longer distances and create larger angles. Increasing the LT decreased the DRA as more powder passed through the larger gap between recoater and substrate; in other words, at larger LTs, there is less powder pile in front of the recoater. Consequently, this lower amount of powder in front of the recoater results in smaller DRAs. The influences of RV and LT on DRA agree with the results on the proposed powder spreadability metric, i.e., deploying lower RV and larger LT led to higher powder spreadability and lower DRA, although

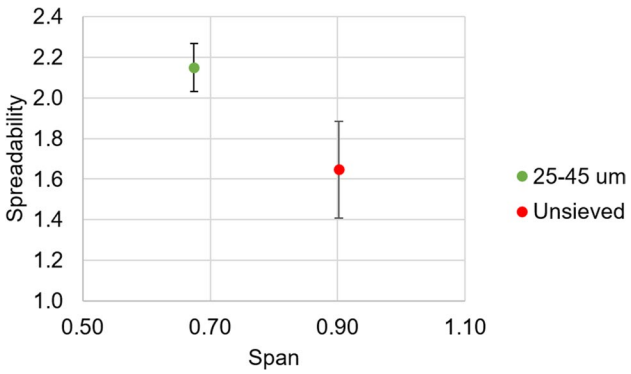

Fig. 7 Effect of size span on powder spreadability

the impact of RV on both metrics was more considerable than that of LT.

Performing an ANOVA with a significance level of 0.05 on the DRA results showed that they are significantly different (P-value < 0.0001). Evaluating the effects of variable factors, as in Table 5, showed a significant interaction between the RV and LT (P-value = 0.0016), i.e., RV and LT are interdependently affecting the DRA. Also, the main effect tests indicated that both RV and LT are significant factors in determining the DRA.

3.2.2 Impact of particle size distribution on dynamic repose angle

The impact of PSD on DRA is shown in Fig. 9. The more uniform 25–45 powder with a narrower span showed higher spreadability with smaller DRA, while increasing the size span led to lower spreadability and larger DRA. This behavior can be explained by the higher cohesivity of powder with wider PSD. The Van der Waals forces exerted by smaller particles overcome their gravity forces; thus, the smaller particles are more willing to agglomerate. In addition, the heavier weight of larger particles forces them to stay still. These circumstances provide required conditions for the smaller particles to agglomerate around the larger particles, creating a cohesive powder with low powder bed density, high surface roughness, and large DRA.

3.3 Correlation between spreadability and dynamic repose angle

After experimenting the impact of recoating velocity and layer thickness on two metrics of powder spreadability and dynamic repose angle, it is necessary to investigate the correlation between these two metrics, i.e., whether spreadability shows similar behavior as dynamic repose angle under the same spreading conditions. Therefore, the correlation between spreadability and dynamic repose angle was evaluated, and the results are shown in Fig. 10. As the correlation coefficient R is very close to 1 (0.94), the spreadability and dynamic repose angle are very similar functions of RV and LT. Also, the R^2 being close to 1 (0.89) indicates that the results can be well fitted to a linear relationship. This great correlation shows that these two metrics can be interchangeably used depending on their ease of use for different applications. It also should be noted that the correlation between spreadability and dynamic response angle is inversely proportional, as a more spreadable powder (higher values of spreadability) results in a smaller repose angle.

Table 5 Evaluation of interaction term and main effects of recoating velocity and layer thickness on dynamic repose angle

Source	DF	Sum of squares	F ratio	Prob > F
LT (um)	2	2.768678	3831.010	< .0001*
RV (%)	3	29.014567	26764.90	< .0001*
LT (um)*RV (%)	6	0.011115	5.1267	.0016*

4 Conclusion

The dependence of powder spreadability and dynamic repose angle (DRA) on the spreading process parameters showed that a significantly higher powder spreadability was obtained with lower recoating velocity (RV) due to the more organized particle motion caused by slower speed and less momentum. Layer thickness (LT) also had a statistically significant effect on powder spreadability, where larger LT slightly improved the powder spreadability as more powder was packed underneath the recoater. In addition, larger particle size with a narrower span led to higher spreadability. The heavier weight of larger particles overcame the Van der Waals forces, forcing the particles to deposit in the

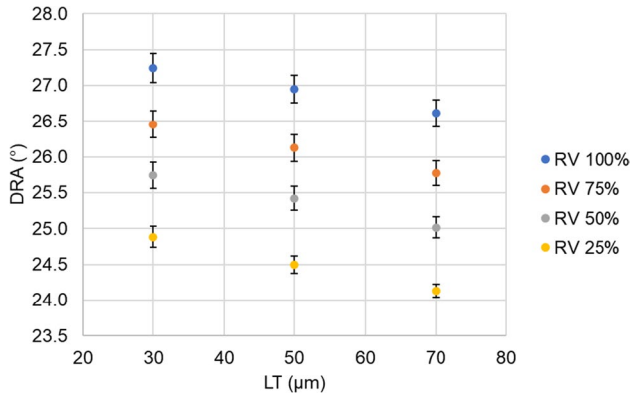

Fig. 8 Effect of recoating velocity and layer thickness on dynamic repose angle

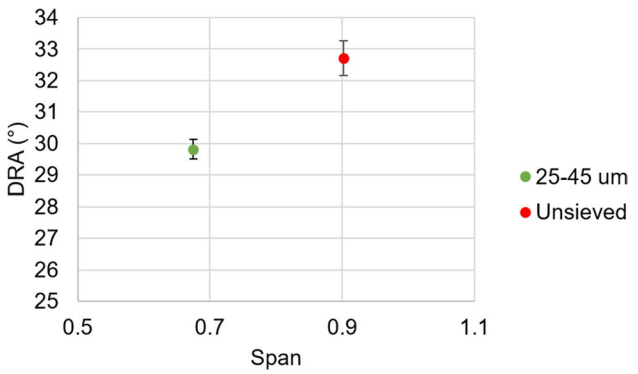

Fig. 9 Effect of size span on DRA

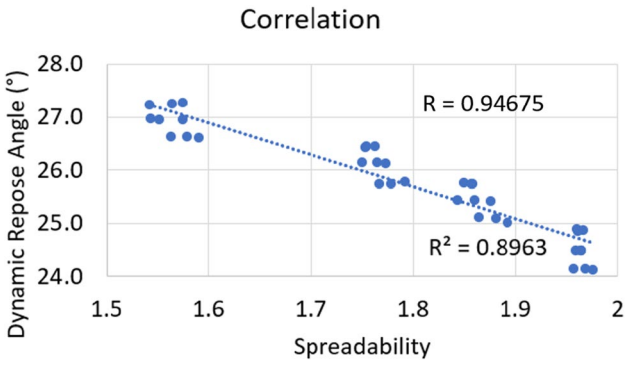

Fig. 10 Correlation relationship between spreadability and dynamic repose angle

substrate at an early stage. For the powder with a wide span, the existence of light-weight smaller particles mixed with larger particles increased the interparticle Van der Waals forces, agglomerating the smaller particles around the larger ones, increasing the powder cohesivity, and deteriorating the powder spreadability due to the decreased powder bed density and the increased surface roughness. A high correlation was observed between the spreadability and DRA as they have strong correlation under different spreading parameters; the value of DRA decreases as the spreadability increases. Therefore, DRA can be used as a spreadability index.

Acknowledgements The publisher, by accepting the article for publication, acknowledges that the US government retains a nonexclusive, paid-up, irrevocable, worldwide license to publish or reproduce the published form of this manuscript, or allow others to do so, for the US government purposes.

Author contribution Conceptualization: M. Hossein Sehhat and Austin T. Sutton. Data curation: M. Hossein Sehhat and Zane Yates. Investigation: M. Hossein Sehhat, Zane Yates, and Ming C. Leu. Formal analysis: M. Hossein Sehhat. Funding acquisition: Ming C. Leu. Writing (original draft): M. Hossein Sehhat. Writing (review and editing): M. Hossein Sehhat and Ming C. Leu.

Funding This work was funded by Honeywell Federal Manufacturing & Technologies LLC under Contract No. DE-N000343667 with the US Department of Energy.

Data availability The raw/processed data required to reproduce these findings will be made available upon request.

Declarations

Conflict of interest The authors declare no competing interests.

References

1. Sehhat MH, Mahdianikhotbesara A, Hadad M (2022) Formability investigation for perforated steel sheets. SAE Int J Mater Manuf 5(2):175–186. https://doi.org/10.4271/05-15-02-0012
2. Mahdianikhotbesara A, Sehhat MH, Hadad M (2021) Experimental study on micro-friction stir welding of dissimilar butt joints between Al 1050 and pure copper. Metallogr Microstruct Anal 2021:1–16. https://doi.org/10.1007/S13632-021-00771-5
3. Mahdianikhotbesara A, Sehhat MH, Hadad M (2022) A numerical and experimental study into thermal behavior of micro friction stir welded joints of Al 1050 and copper sheets. Adv Mater Res 1170:49–60. https://doi.org/10.4028/P-01AG12
4. Turk T, Hung C-H, Hossein Sehhat M, Leu MC (2021) Methods of automating the laser-foil-printing additive manufacturing process, 2021. In: International solid freeform fabrication symposium. The University of Texas, Austin. https://repositories.lib.utexas.edu/handle/2152/90714
5. Hadad M, Gholampour Darzi J, Mahdianikhotbesara A, Makarian J (2022) Experimental investigation of the effect of single point dressing parameters on grinding of Mo40 hardened steel using mounted point grinding tool, Energy Equip. Syst 10:197–214. https://doi.org/10.22059/EES.2022.253231
6. Chenarani V, Mahdianikhotbesara A, Hadad M, Sehhat MH, Hedayati-Dezfooli M, Zaheri A, Araee A (2022) Evaluation of the forming limit diagram (FLD) for St-Mg-St multilayer sheet manufactured by transient liquid phase (TLP) bonding. Metallogr Microstruct Anal 2022:1–13. https://doi.org/10.1007/S13632-022-00904-4
7. Liu T, Lough CS, Sehhat H, Ming Y, Christofides PD, Kinzel EC, Leu MC (2022) In-situ infrared thermographic inspection for local powder layer thickness measurement in laser powder bed fusion. Addit Manuf 55:102873. https://doi.org/10.1016/j.addma.2022.102873
8. Liu T, Lough CS, Sehhat H, Huang J, Kinzel EC, Leu MC (2021) In-situ thermographic inspection for laser powder bed fusion, 2021. In: International Solid Freeform Fabrication Symposium. University of Texas, Austin. https://repositories.lib.utexas.edu/handle/2152/90637
9. Behdani B, Senter M, Mason L, Leu M, Park J (2020) Numerical study on the temperature-dependent viscosity effect on the strand shape in extrusion-based additive manufacturing. J Manuf Mater Process 4:46. https://doi.org/10.3390/jmmp4020046
10. Yigit IE, Isa M, Lazoglu I (2018) Additive manufacturing with modular support structures, 2018. In: International Solid Freeform Fabrication Symposium. University of Texas, Austin. https://doi.org/10.26153/TSW/17208
11. Isa MA, Yiğit IE, Lazoglu I (2018) Analysis of build direction in deposition-based additive manufacturing of overhang structures, 2018. In: International Solid Freeform Fabrication Symposium. University of Texas, Austin. https://doi.org/10.26153/TSW/17156.
12. Sehhat MH, Behdani B, Hung CH et al (2021) Development of an empirical model on melt pool variation in laser foil printing additive manufacturing process using statistical analysis. Metallogr Microstruct Anal 10:684–691. https://doi.org/10.1007/s13632-021-00795-x
13. Hung C-H, Chen W-T, Sehhat MH, Leu MC (2021) The effect of laser welding modes on mechanical properties and microstructure of 304L stainless steel parts fabricated by laser-foil-printing additive manufacturing. Int J Adv Manuf Technol 112:867–877
14. Hung C-H, Turk T, Sehhat MH, Leu MC (2022) Development and experimental study of an automated laser-foil-printing additive manufacturing system. Rapid Prototyp J ahead-of-print. https://doi.org/10.1108/RPJ-10-2021-0269
15. Sehhat MH, Mahdianikhotbesara A, Yadegari F (2022) Impact of temperature and material variation on mechanical properties of parts fabricated with fused deposition modeling (FDM) additive manufacturing. Int J Adv Manuf Technol. https://doi.org/10.1007/S00170-022-09043-0
16. Sehhat MH, Mahdianikhotbesara A, Yadegari F (2022) Verification of stress transformation in anisotropic material

additively manufactured by fused deposition modeling (FDM). Int J Adv Manuf Technol 2022:1–7. https://doi.org/10.1007/S00170-022-10321-0
17. Turk T, Leu MC (2023) Experimental study for improving the productivity of laser foil printing. Int J Adv Manuf Technol 2023. https://doi.org/10.1007/s00170-023-11076-y
18. Rafi AH, Lakusta M, Anthony V, Basler G, Grier S, Moeller L, Lipke D, Watts JL, Hilmas G, Leu MC (2022) Ceramic on-demand extrusion of ZrB2-SiC microchannels for ultra high-temperature compact heat exchanger, 2022. In: International solid freeform fabrication symposium. University of Texas, Austin. https://repositories.lib.utexas.edu/handle/2152/117256
19. Sehhat MH, Chandler J, Yates Z (2022) A review on ICP powder plasma spheroidization process parameters. Int J Refract Met Hard Mater 103:105764. https://doi.org/10.1016/J.IJRMHM.2021.105764
20. Sehhat MH, Sutton A, Leu M (2022) Enhancement of gas-atomized 304l stainless steel powder by plasma spheroidization for use in the laser powder bed fusion process. U.S. Department of Energy,Office of Scientific and Technical Information. https://doi.org/10.2172/1876883
21. Sehhat MH, Perez-Palomino D, Wiedemeier C, Cullom T, Newkirk JW, Leu MC (2023) Characterization of virgin, re-used, and oxygen-reduced copper powders processed by the plasma spheroidization process. Adv Powder Technol34(1):103885. https://doi.org/10.1016/j.apt.2022.103885
22. Rafi AH, Ahmed DH (2022) Two-dimensional analogies to the deformation characteristics of a falling droplet and its collision. Arch Mech Eng 69(1). https://doi.org/10.24425/ame.2021.139649
23. Kundakcioglu E, Lazoglu I, Rawal S (2015) Transient thermal modeling of laser-based additive manufacturing for 3D freeform structures. Int J Adv Manuf Technol 851(85):493–501. https://doi.org/10.1007/S00170-015-7932-2
24. Kundakcıoğlu E, Lazoglu I, Poyraz Ö, Yasa E, Cizicioğlu N (2018) Thermal and molten pool model in selective laser melting process of Inconel 625. Int J Adv Manuf Technol 959(95):3977–3984. https://doi.org/10.1007/S00170-017-1489-1
25. Khan SA, Lazoglu I (2019) Development of additively manufacturable and electrically conductive graphite–polymer composites. Prog Addit Manuf 52(5):153–162. https://doi.org/10.1007/S40964-019-00102-9
26. Roshan A, Ahmadi M, Domiri Ganji D (2022) Variational Iteration Method (VIM) and Parameter Perturbation Method (PPM) for the Solution of nonlinear differential equation of beam elastic deformation. Southeast Asian Bulletin of Mathematics 46:35–44
27. Sehhat MH, Sutton AT,Hung CH, Brown B, O'Malley R, Park J, Leu MC (2022) Plasmaspheroidization of gas-atomized304L stainless steel powder forlaser powder bed fusion process.Mater Sci Add Manuf 1(1):1.https://doi.org/10.18063/msam.v1i1.1
28. Isa MA, Lazoglu I (2019) Five-axis additive manufacturing of freeform models through buildup of transition layers. https://doi.org/10.1016/j.jmsy.2018.12.002
29. Yigit IE, Lazoglu I (2019) Helical slicing method for material extrusion-based robotic additive manufacturing. Prog Addit Manuf 4:225–232. https://doi.org/10.1007/s40964-019-00090-w
30. Yigit IE, Lazoglu I (2020) Spherical slicing method and its application on robotic additive manufacturing. Prog Addit Manuf 54(5):387–394. https://doi.org/10.1007/S40964-020-00135-5
31. Sehhat MH, Sutton AT, Hung C-H, Newkirk JW, Leu MC (2021) Investigation of mechanical properties of parts fabricated with gas- and water-atomized 304L stainless steel powder in the laser powder bed fusion process. JOM 1:8. https://doi.org/10.1007/S11837-021-05029-7
32. Nezhadfar PD, Thompson S, Saharan A, Phan N, Shamsaei N (2021) Structural integrity of additively manufactured aluminum alloys: effects of build orientation on microstructure, porosity, and fatigue behavior. Addit Manuf 47:102292. https://doi.org/10.1016/J.ADDMA.2021.102292
33. Nezhadfar PD, Shamsaei N, Phan N (2021) Enhancing ductility and fatigue strength of additively manufactured metallic materials by preheating the build platform. Fatigue Fract Eng Mater Struct 44:257–270. https://doi.org/10.1111/FFE.13372
34. Nezhadfar PD, Thompson S, Saharan A, Phan N, Shamsaei N (2021) Fatigue and failure analysis of an additively manufactured contemporary aluminum alloy. In: Perander L (ed) Light Metals 2021. The Minerals, Metals & Materials Series. Springer, Cham. https://doi.org/10.1007/978-3-030-65396-5_31
35. Sehhat MH, Mahdianikhotbesara A (2021) Powder spreading in laser-powder bed fusion process. Granul Matter 23:89. https://doi.org/10.1007/s10035-021-01162-x
36. Ahmed M, Pasha M, Nan W, Ghadiri M (2020) A simple method for assessing powder spreadability for additive manufacturing. Powder Technol 367:671–679. https://doi.org/10.1016/j.powtec.2020.04.033
37. Cordova L, Bor T, de Smit M, Campos M, Tinga T (2020) Measuring the spreadability of pre-treated and moisturized powders for laser powder bed fusion. Add Manuf 32:101082.https://doi.org/10.1016/j.addma.2020.101082
38. Zhang J, Tan Y, Bao T, Xu Y, Xiao X, Jiang S (2020) Discrete element simulation of the effect of roller-spreading parameters on powder-bed density in additive manufacturing. Materials 13(100):2285. https://doi.org/10.3390/ma13102285
39. Parteli EJR, Pöschel T (2015) Particle-based simulation of powder application in additive manufacturing. Powder Technol 288:96–102. https://doi.org/10.1016/j.powtec.2015.10.035
40. Macho O, Demková K, Gabrišová Ľ, Čierny M, Mužíková J, Galbavá P, Nižnanská Ž, Blaško J, Peciar P, Fekete R, Peciar M (2020) Analysis of static angle of repose with respect to powder material properties. Acta Polytech 60:73–80. https://doi.org/10.14311/AP.2020.60.0073
41. Roshan A, Shooshpasha I (2014) Numerical Analysis Of Piled Raft Foundations In Soft Clay International Journal For Numerical And Analytical Methods In Geomechanics, vol 22
42. Schneider CA, Rasband WS, Eliceiri KW (2012) NIH Image to ImageJ: 25 years of image analysis. Nat Methods 97(9):671–675. https://doi.org/10.1038/nmeth.2089
43. Chen H, Wei Q, Zhang Y, Chen F, Shi Y, Yan W (2019) Powder-spreading mechanisms in powder-bed-based additive manufacturing: experiments and computational modeling. Acta Mater 179:158–171. https://doi.org/10.1016/j.actamat.2019.08.030